Experimental In-Body to On-Body and In-Body to In-Body Path Loss Models of Planar Elliptical Ring Implanted Antenna in the Ultra-Wide Band

Xiao Fang[1], Mehrab Ramzan[1], Qiangbo Zhang[1], Sofia Pérez-Simbor[2], Qiong Wang[1], Niels Neumann[1], Concepcion Garcia-Pardo[2], Narcís Cardona[2] and Dirk Plettemeier[1]

[1]Chair of RF Engineering, Communication laboratory, TU Dresden, Dresden, Germany
[2]Institute of Telecommunications and Multimedia Applications,UniversitatPolitècnica de València,Valencia, Spain

Abstract—**This paper presents in-body to on-body and in-body to in-body channel models of a planar wideband elliptical ring implanted antenna in the lower part of Ultra-WideBand (UWB, 3.1 to 5.1 GHz). The results are verified inside a practical UWB liquid phantom with the help of a wideband on-body monopole antenna. Moreover, the design principle of the in-body and on-body antennas, as well as their simulated and measured reflection coefficients are presented. The channel characterization inside the lossy medium gives a deep insight of wireless capsule endoscope technology (WCE) and helps to evaluate the radiation performance of the previously designed planar elliptical ring implanted antenna.**

Keywords—Implanted antennas, Path Loss,UWB band, Phantoms, Elliptical Antenna, On-body antennas, Wireless Capsule Endoscope (WCE), Body area communication

I. INTRODUCTION

In the last few years, WCE technology has become popular replacing the traditional wired endoscopy which may cause complications for the patients in the field of medicine and surgery [1-3]. The non-invasive way of examination in a WCE scenario is shown in Fig. 1. There is an in-body wireless capsule moving continuously inside the Gastrointestinal (GI) tract of the human stomach wirelessly transmiting the examination data to the on-body receiver antenna. The bandwidth limitations at lower frequencies such as MICS band and 2.4 GHz ISM band do not suffice the requirements of high resolution images for the medical meticulous examination of the GI tract due to the high data rate requirement of this technology, [4-6]. Therefore, UWB is the possible potential frequency band which does not only provide high quality images, but it also enables low output power technology which is a critical concern for the wireless implanted devices according to the regulatory bodies for human protection [7]. It is essential to accurately understand the propagation loss mechanisms between the in-body and on-body antenna. The wireless capsule taken by the patients interact with different human organs having different electrical properties which deviate the resonance frequency of the antenna [8, 9]. The antenna is the key component in this wireless capsule technology that needs proper designing and examination before being deployed.

In this paper, we propose in-body to on-body and in-body to in-body channel models for GI application based on WCE which give an insight of the propagation losses inside the lossy human body tissues. The channel models are based on a planar elliptical ring in-body antenna that covers the lower frequency part of UWB. For the on-body receiver, we propose a wideband semi-circle monopole antenna working from 3 GHz to 5 GHz.

The paper is organized into four sections. The first section gives a brief overview and measured reflection coefficient results of the in-body and on-body antennas, as well as the radiation patterns of the in-body and on-body antennas. The second section illustrates the experimental channel model of in-body to on-body communication scenario. In the third section the channel characteristics of the in-body to in-body measurement setup are discussed. Finally the conclusion of the paper is given.
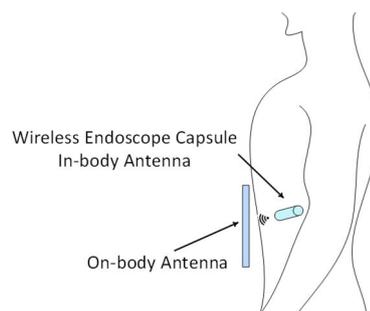

Fig. 1. The diagram of Wireless Endoscope Capsule communication.

II. ANTENNAS

A. In-body Antennas

The in-body antennas are planar elliptical ring implanted antennas working at the lower part of UWB frequency band. They have small dimensions that enable them to be embedded in a wireless capsule and be easily swallowed by the patients through the esophagus. The antennas are fabricated on 75-mil-thick circular shape Rogers TMM10 substrate with the radius of 5.85 mm. The top layer of the substrate is a double elliptical ring while on the bottom layer is the ground plane. In order to measure the antennas, 50-ohm coaxial cables are utilized to connect the antenna with a Vector Network Analyzer (VNA). Fig. 2(a) shows the fabricated antennas and Fig. 2(b) depicts the antennas with coaxial cables. The simulation and measurement of S11 results are shown in Fig. 3 inside the phantom. The simulation environment is homogeneous muscle phantom with relativity permittivity ε_r of 52.2 and conductivity of 3.3, in which the designed in-body antenna is immersed. For the measurement, the electrical properties of the phantom are also similar with human muscle tissue. As illustrated in Fig. **3**, the reflection coefficients are below -

10 dB for the whole required frequency band (3.1 GHz – 5.1 GHz), and the measurement results agree well with the simulation results. Fig. 4 and Fig. 5 show the radiation patterns of the antenna inside the phantom. More details about the structure and radiation characteristics of the in-body antenna can be found in [8].

Fig. 2. Fabricated in-body antennas *(a)* antennas without coaxial cable. *(b)* antennas with coaxial cable.
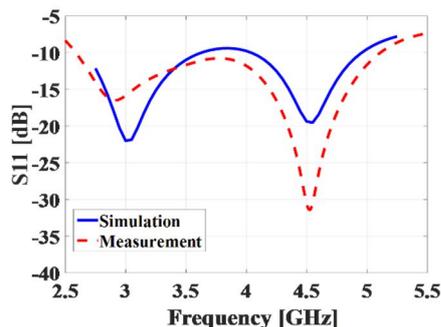

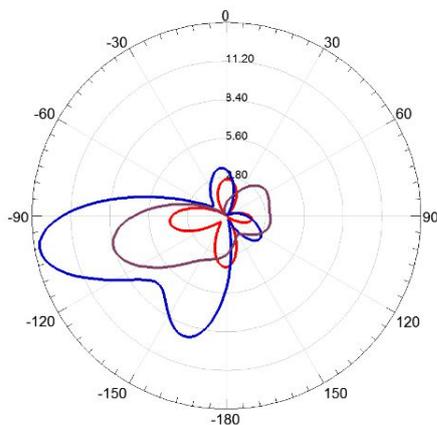Fig. 3. Measured and simulated reflection coefficient results of in-body antenna inside the muscle phantom.

Fig. 4. Simulated radiation patterns (phi = 90 deg) of the in-body antenna at 3 GHz, 4 GHz and 5GHz inside the muscle phantom.
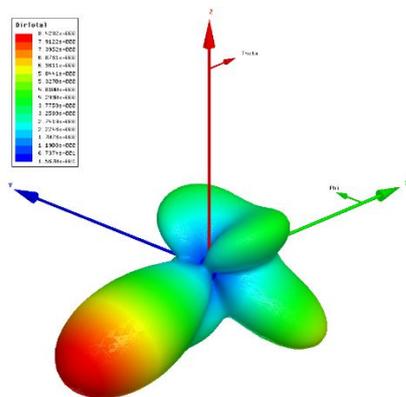

Fig. 5. 3D view of simulated radiation pattern of the in-body antenna at 4 GHz inside the muscle phantom.

B. On-body Antennas

Additionally, an on-body antenna is designed to measure the in-body to on-body transmission. Fig. 6 shows the fabricated on-body antenna which is designed based on RO3203 substrate with the relative permittivity of 3.02. The dimensions of the antenna are 40 mm x 40 mm. Due to its low profile, miniaturized and light weight features, the antenna can be easily integrated with the on-body electric devices. Fig. 6 (a) shows the top layer of the antenna consisting of a semicircular part and microstrip line. The top semicircular part is the radiating element of the antenna which has a wideband characteristic. Fig. 6 (b) illustrates the bottom layer of the antenna which is the ground plane. The trapezoidal shape is used to tune the input impedance to 50 ohms. As shown in Fig. 7, due to the thickness of wall of cabinet of phantom, in the whole frequency band the measurement S11 doesn't totally agree with the simulated S11. From the measurement results, we can see that the fabricated antenna is well matched (S11<-10 dB) within the lower part of the UWB band. The simulated radiation patterns of the antenna at 3 GHz, 4 GHz and 5 GHz in free space are shown in Fig. 8, as well as in Fig. 9 which gives the 3D view of radiation pattern at 4 GHz. It is obvious that the radiation patterns of the designed on-body antenna are similar to that of a dipole and remain constant over all the desired frequency bands.
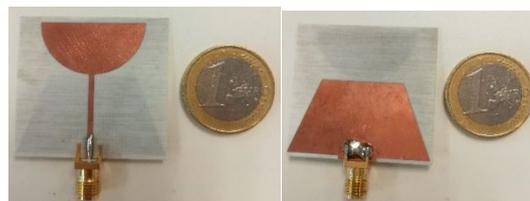

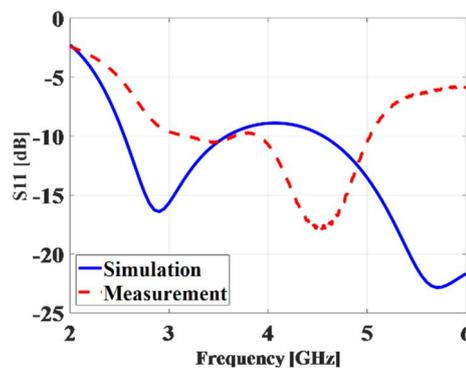Fig. 6. Fabricated on-body antennas *(a)* Front side of antenna. *(b)* Back side of the antenna.

Fig. 7. Measured and simulated reflection coefficient results of on-body antenna on the muscle phantom.
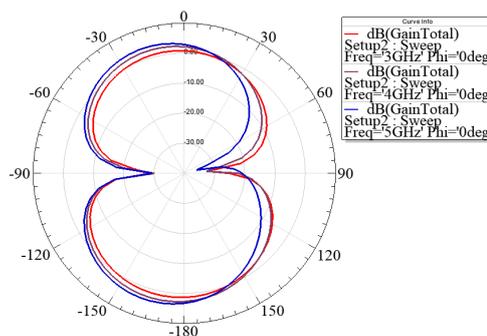

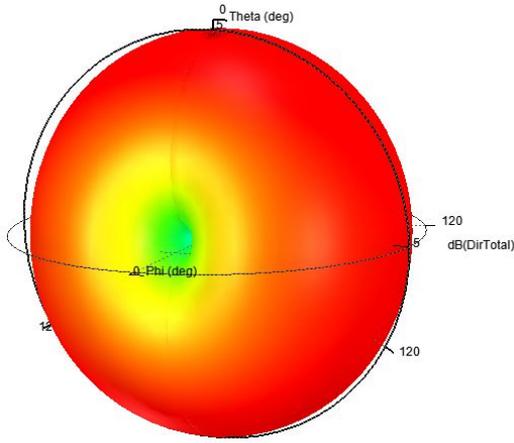Fig. 8. Simulated radiation patterns (phi = 90 deg) of the on-body antenna at 3 GHz, 4 GHz and 5GHz in free space,

Fig. 9. 3D view ofsimulated radiation pattern of the on-body antenna at 4 GHz in free space.

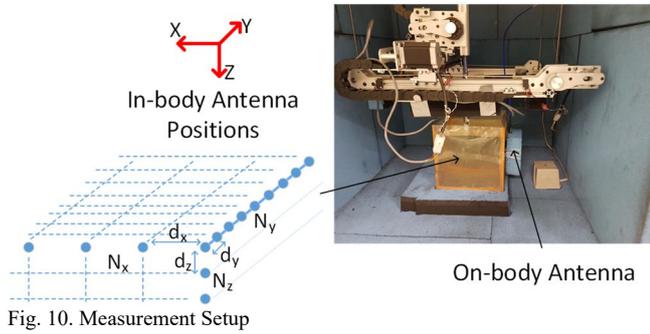## III. MEASURED IN-BODY TO ON-BODY PATH LOSS MODELS

Fig. 10. Measurement Setup

The channel model measurements are carried out inside a small anechoic chamber with its boundaries covered with absorbing materials, similar to the setup in [10], as shown in Fig. 10. The measurement setup consists of 250 mm × 250 mm × 250 mm box containing the UWB liquid phantom which is developed on the basis of sugar and salt recipe composition in order to mimic the electrical properties of the human muscle [11]. A robotic arm mounted with in-body antenna is used for the automatic changing of the position of the in-body antenna precisely inside the liquid phantom. In the in-body to on-body channel modeling case as shown in Fig. 10, the in-body antenna was set up to N_x=6, N_y=8 and N_z =3 which are the number of measured points in x, y and z direction, and with their corresponding step size of dx=1 cm, dy= 1 cm and dz=1 cm in x, y and z direction, respectively. The positions of the on-body antenna are changed manually on the surface of the cabinet. In this case, two positions of the on-body antenna are measured.

The transmission coefficient (S21) between the in-body antenna and the on-body antenna per position is obtained from the measurement setup. The S21 versus frequency points are utilized to calculate the mean path loss value of the full bandwidth.

$$PL_{dB} = -10\log(\sum_{i=N} \frac{|S21(f_i)|^2}{N}) \qquad (1)$$

f_i represents the frequency points from 3.1 GHz to 5.1 GHz. N is the number of the measured frequency points which is 1601. The path loss values at different positions are shown in Fig. 11. The separation distance is changed from 60 mm to

110 mm and the corresponding path loss values are recorded to be between 65 dB and 95 dB which are acceptable values by typical GI tract devices. The log-normal path loss model is utilized to fit the mean path loss values as shown in Fig. 11. The amplitude variation of the measured path loss values around the fitted mean path loss is around 5 dB, which is due to the diffraction in the shadowed regions of the utilized cabinet as well as the reflection from the robotic arm and the wall of the anechoic chamber. It can be modeled using a log-normal distribution with a standard deviation. The in-body to on-body path loss model is combination of both the statistical variance of path loss and the fitted mean path loss, which can be written as:

$$PL_{dB}(d) = PL_{0,dB} + 10n\log_{10}\left(\frac{d}{d_0}\right) + N(0,\sigma_{dB}) \quad (2)$$

Where $PL_{0,dB}$ is the path loss at the reference distance d_0 and n is the path loss exponent. The cumulative distribution function (CDF) is approximated by a log normally distributed random variable $N(0,\sigma_{dB})$ with zero mean and standard deviationσ_{dB}. σ_{dB} reflects the concentration of the path loss around its mean value as well as the degree of diffraction and reflection [9]. Fig. 12 shows the measured and fitted CDF of normal distribution. The standard deviation is fitted at $\sigma_{dB} = 2.2\ dB$, which implies the variance of the path loss values because of the reflection and diffraction. All the extracted factors of the path loss model are summarized in Table I.
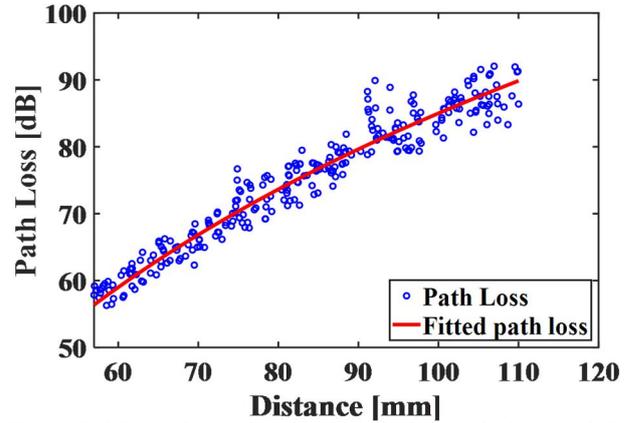

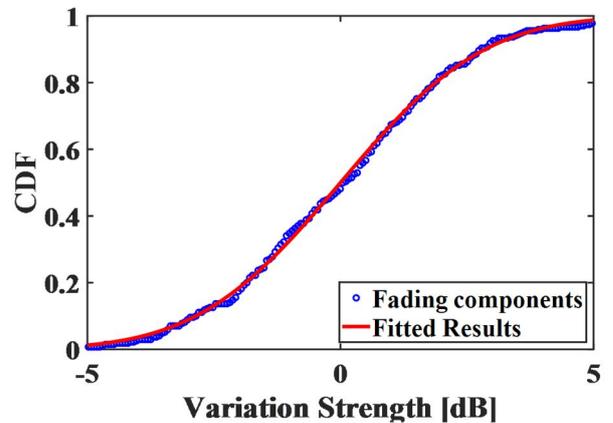Fig. 11. Path loss values and models for in-body to on-body transmission at lower part of UWB band.

Fig. 12. CDF of variation strength for in-body to on-body transmission at lower part of UWB band.

TABLE I.   IN-BODY TO ON-BODY PATH LOSS MODELS

In-body to On-body Path Loss Models				
$PL_{0,dB}$	d_0	d	n	σ
59 dB	60 mm	[57, 110] mm	11.7	2.2

IV.   MEASURED IN-BODY TO IN-BODY PATH LOSS MODELS

As discussed in some papers [12, 13], the radiation characteristics of the antenna inside the lossy medium cannot be evaluated using the definition of radiation characteristics of antennas in free space. Thus, in order to evaluate the radiation performance of the designed implanted antenna in lossy medium, the in-body to in-body transmission performance of the elliptical ring antenna is measured. Two planar elliptical ring antennas are used where one of the in-body antenna position is kept constant inside the liquid phantom while the position of the other in-body antenna attached to the robotic arm is changed. The in-body to in-body measurement setup is same as in the previous case shown in Fig. 10.

In Fig. 13, the path loss values are also fitted with log-normal path loss model and the amplitude variation of the measurement path loss values is approximately 10 dB larger than measured in-body to on-body transmission because the in-body antenna is not omnidirectional as shown in Fig. 4 and Fig. 5. As well as the radiation pattern of the antenna related with the distance between antenna and observed point (in this case it is another in-body antenna). As implies in [12, 13], if the antenna is surrounded by the conducting medium, such as muscle phantom, the radiation pattern of the antenna will change with the size of phantom because of the high lossy property of the medium

Based on Equ. (2), the in-body to in-body path loss models also combine the statistical variance of the path loss and the fitted mean path loss. The distance between two antennas is varied from 18 mm to 61mm with path loss values from 42 dB to 72 dB. The reference distance is 20 mm with $PL_{0,dB} = 48\,dB$. The fitted standard deviation σ_{dB} is 2.9. All the parameters of the path loss model are summarized in Table II.
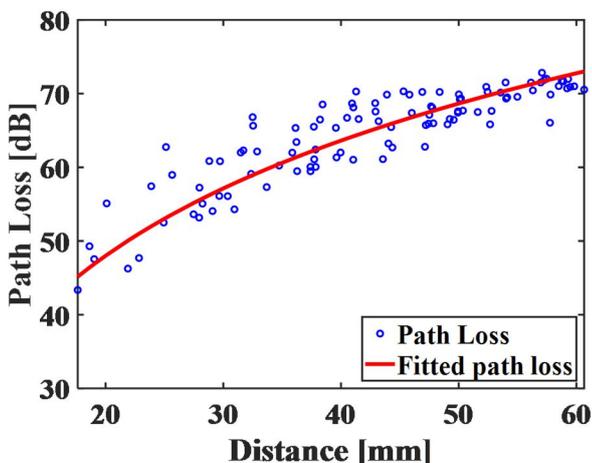

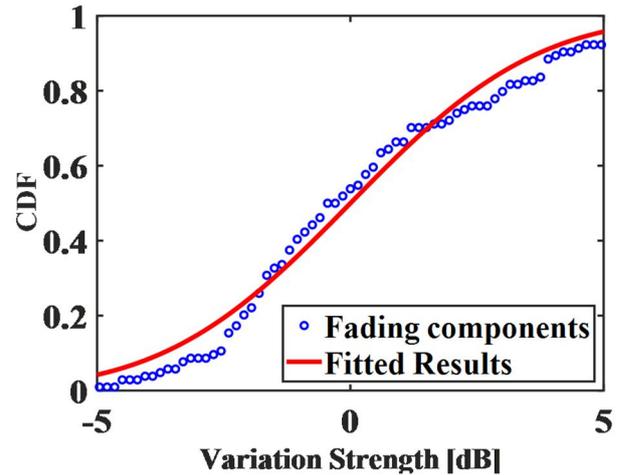Fig. 13. Path loss values and models for in-body to in-body transmission at lower part of UWB band.

Fig. 14. CDF of variation strength for in-body to in-body transmission at lower part of UWB band.

TABLE II.   IN-BODY TO IN-BODY PATH LOSS MODELS

In-body to In-body Path Loss Models				
$PL_{0,dB}$	d_0	D	n	σ
48 dB	20 mm	[18, 61] mm	5.2	2.9

CONCLUSION

In this paper, we discuss the in-body to on-body and in-body to in-body channel modeling inside a UWB liquid phantom for wireless capsule endoscopy based on a planar elliptical in-body antenna and semicircle monopole on-body antenna. These practical channel models in the lossy medium provide a fundamental basis for system design evaluations of WCE technology. These models also confirm the radiation performance of the designed in-body antenna. In future, these antennas will be further used to investigate channel models during an animal experiment in order to compare the in-vitro and in-vivo experiments.

ACKNOWLEDGMENT

REFERENCES

[1]   Yuce, Mehmet R., and Tharaka Dissanayake, "Easy-to-swallow wireless telemetry," IEEE Microwave magazine, vol.13, no.6, pp. 90-101, 2012

[2]   Yuce, R. Yuce, T. Dissanayake, and H. Chee Keong, "Wireless telemetry for electronic pill technology," in Proc. IEEE Conf. Sensors, Oct. 2009, pp.1433–1438.

[3]   Karargyris, Alexandros, and Anastasios Koulaouzidis, "OdoCapsule: next-generation wireless capsule endoscopy with accurate lesion localization and video stabilization capabilities," IEEE Transactions on Biomedical Engineering, vol.62, no.1, pp. 352-360, 2015.

[4]   G. Ciuti, A. Menciassi, and P. Dario, "Capsule endoscopy: from current achievements to open challenges," Biomedical Engineering, IEEE Reviews in, vol. 4, pp. 59–72, 2011.

[5]   W. G. Kwack and Y. J. Lim,"Current Status and Research into Overcoming Limitations of Capsule Endoscopy." Clinical endoscopy, vol. 49, no. 1, pp. 8-15, 2016.

[6] M. Basar, F. Malek, K. Juni, M. Idris and M. Saleh, "Ingestible Wireless Capsule Technology: A Review of Development and Future Indication", International Journal of Antennas and Propagation, vol. 2012, pp. 1-14, 2012.

[7] G. Breed, "A summary of fcc rules for ultra wideband communications," High Frequency Electronics, vol. 4, no. 1, pp. 42–44, 2005.

[8] Q. Zhang, X. Fang, Q. Wang, and D. Plettemeier, "Planar Elliptical Ring Implanted Antennas for UWB Body Area Communication," International Conference on Body Area Networks, BodyNets 2018.

[9] Wang J, Wang Q. Body area communications: channel modeling, communication systems, and EMC[M]. John Wiley & Sons, 2012.

[10] S. P. Simbor, M. Barbi, M. Ramzan, X. Fang, C. Garcia-Pardo, N. Cardona, "Experimental Path loss models comparison and localization of Wireless Endoscopic Capsule in the Ultra Wideband Frequency Band," International Conference on Body Area Networks, BodyNets 2018

[11] Andreu, Carlos, et al. "Spatial in-body channel characterization using an accurate UWB phantom." IEEE Transactions on Microwave Theory and Techniques 64.11,pp. 3995-4002, 2016.

[12] Moore R. "Effects of a surrounding conducting medium on antenna analysis". IEEE Transactions on Antennas and Propagation,11(3), pp. 216-225, 1963.

[13] Skrivervik A K.,"Implantable antennas: The challenge of efficiency", Antennas and Propagation (EuCAP), 2013 7th European Conference on. IEEE, pp. 3627-3631, 2013.